nature COMMUNICATIONS

ARTICLE

DOI: 10.1038/s41467-017-02120-z OPEN

Multiyne chains chelating osmium via three metal-carbon σ bonds

Qingde Zhuo[1], Jianfeng Lin[1], Yuhui Hua[1], Xiaoxi Zhou[1], Yifan Shao[1], Shiyan Chen[1], Zhixin Chen[1], Jun Zhu[1], Hong Zhang[1] & Haiping Xia[1]

Although the formation of metal–carbon σ bonds is a fundamental principle in organometallic chemistry, the direct bonding of one organic molecule with one metal center to generate more than two metal–carbon σ bonds remains a challenge. Herein, we report an aromaticity-driven method whereby multiyne chains are used to construct three metal–carbon σ bonds in a one-pot reaction under mild conditions. In this method, multiyne chains act as ligand precursors capable of chelating an osmium center to yield planar metallapolycycles, which exhibit aromaticity and good stability. The direct assembly of various multiyne chains with commercially available metal complexes or even simple metal salts provides a convenient and efficient strategy for constructing all carbon-ligated chelates on the gram scale.

[1] State Key Laboratory of Physical Chemistry of Solid Surfaces and Collaborative Innovation Center of Chemistry for Energy Materials (iChEM), College of Chemistry and Chemical Engineering, Xiamen University, Xiamen 361005, China. Correspondence and requests for materials should be addressed to H.X. (email: hpxia@xmu.edu.cn)

The construction of metal–carbon σ bonds is a fundamental process in organometallic chemistry[1, 2]. A large array of organic molecules form a single σ bond with metals, resulting in species such as metal alkyl[3, 4], metal carbene[5–12], and metal carbyne[13–18] complexes. Certain organic molecules can bond with a metal center through two metal–carbon σ bonds, leading to the corresponding bidentate CC-type chelates, such as metallacyclopentadienes[19–25] and metallabenzenes[26–34]. However, the direct σ-bonding of a single organic molecule to a single metal center to form tridentate CCC-type chelates is uncommon. Most of them contain *N*-heterocyclic carbene ligands, which are electron-rich σ-donor ligands that can strongly bond the metal centers in a manner similar to classical 2e donors such as phosphine ligands[35–37]. Another related example is the tantalum complexes derived from 1-iodo-2,6-di-*p*-tolylbenzene through lithiation and cyclometallation processes, in which the terphenyl ligand attaches to a metal center through three metal–carbon single bonds[38].

In recent years, our research has focused on the construction of as many metal–carbon σ bonds as possible between a carbon ligand and a metal center, achieving a series of conjugated carbon-ligated multidentate chelates, termed carbolong complexes, with novel structures and unique properties[39–43]. All of these complexes contain three or more metal–carbon σ bonds; however, these metal–carbon σ bonds could only be constructed step by step.

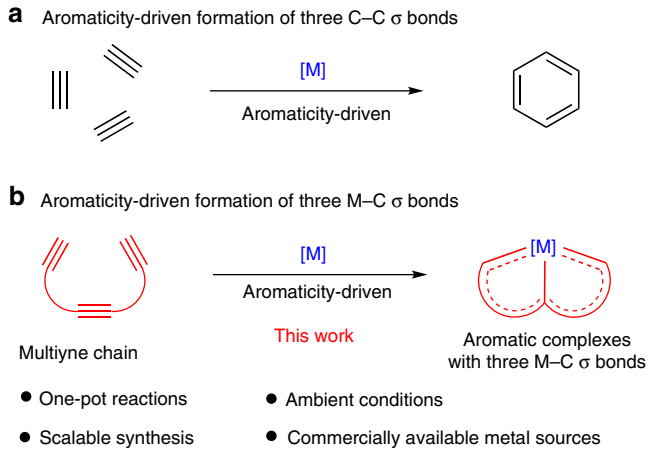

Fig. 1 Efficient synthesis through aromaticity-driven cyclization reactions. **a** Formation of three C–C σ bonds through an aromaticity-driven process. **b** Formation of three M–C σ bonds through an aromaticity-driven process. [M] transition metal and ancillary ligands, M–C metal–carbon

Aromaticity-driven cyclization reactions have been widely used in synthetic chemistry owing to the relatively lower energies of the aromatic products compared to their non-aromatic or anti-aromatic analogs. Numerous aromatic hydrocarbons have been constructed using this method. As shown in Fig. 1a, one of the most prominent examples of this chemistry is the transition metal-catalyzed [2 + 2 + 2] cycloaddition reactions of alkynes, which can form three carbon–carbon σ bonds in a one-pot reaction to obtain benzene and its derivatives[44]. Thus, we considered whether the direct construction of three metal–carbon σ bonds could also be achieved through an aromaticity-driven process. Herein, we present an efficient strategy involving aromaticity-driven processes in a one-pot reaction to achieve stable multidentate complexes containing three metal–carbon σ bonds (Fig. 1b). The direct reaction of multiyne chains with a commercially available metal complex ($OsCl_2(PPh_3)_3$) or even a simple metal salt (K_2OsCl_6) affords all carbon-ligated chelates with both single and multiple metal–carbon bonds under ambient conditions on the gram scale. The promising synthetic potential of this method is evidenced by the extension of the multiynes to produce diverse chelate scaffolds.

Results

Synthesis of CCC-type chelates with three M–C σ bonds. We first designed and prepared the carbon ligand precursor **L1** (Fig. 2a; see Supplementary Methods for synthesis details). **L1** is a triyne chain containing two functional modules (an acetenyl unit and a 3-hydroxyl pentadiynyl unit) connected by a flexible linker. As shown in Fig. 2a, the treatment of **L1** with $OsCl_2(PPh_3)_3$ and PPh_3 in dichloromethane under air at room temperature (RT) for 1 h resulted in the formation of CCC-type chelate **1** with a yield of 82%.

Chelate **1** was characterized by nuclear magnetic resonance (NMR) spectroscopy. The ^{13}C NMR spectrum shows a typical chemical shift of the carbyne carbon in **1** at 321.57 parts per million (ppm). The downfield ^{1}H NMR chemical shifts (H7 at 13.14 ppm and H3 at 7.64 ppm) appear to be diagnostic of the presence of an aromatic framework, which is common for aromatic metallacycles[26–34, 45–47]. Single-crystal X-ray analyses indicated that a tridentate CCC-type ligand was attached to the osmium center by three metal–carbon σ bonds (Fig. 2b), confirming that the combination of **L1** with the osmium substrate led to the conversion of five *sp* carbons and one sp^3 carbon to six sp^2 carbons. The Os–C1 bond length (1.840(7) Å, where the value in parentheses represents the standard deviation) is at the high end of the range for Os≡C triple bonds (1.612–1.856 Å). However, the other two Os–C bond lengths (i.e., 2.108(7) Å for Os–C4 and 2.040(8) Å for Os–C7) are within the range of the

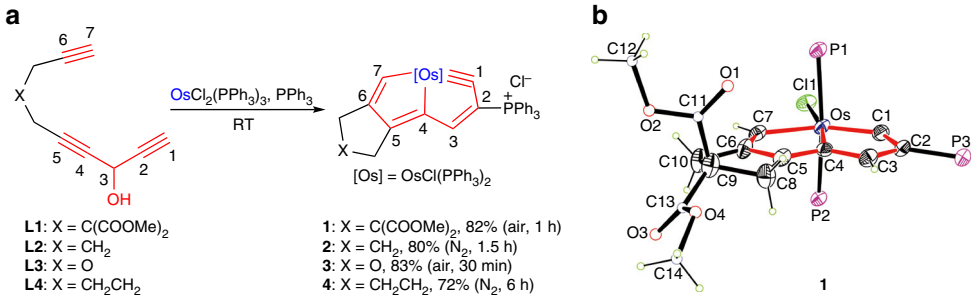

Fig. 2 Synthesis of CCC-type osmium chelates from triynes. **a** Triynes as ligand precursors to access CCC-type chelates with three metal–carbon σ bonds. **b** X-ray structure of the cation of chelate **1** drawn with 50% probability (phenyl groups in PPh_3 are omitted for clarity). Selected bond distances (Å) and angles (deg): Os–C1 1.840(7), Os–C4 2.108(7), Os–C7 2.040(8), C1–C2 1.406(10), C2–C3 1.394(10), C3–C4 1.395(9), C4–C5 1.390(10), C5–C6 1.395(10), C6–C7 1.366(10), Os–C1–C2 129.3(6), C1–C2–C3 108.3(6), C2–C3–C4 112.1(6), C3–C4–Os 117.1(5), C1–Os–C4 73.2(3), Os–C4–C5 116.6(5), C4–C5–C6 113.6(7), C5–C6–C7 115.5(7), C6–C7–Os 118.9(5), C7–Os–C4 75.4(3)

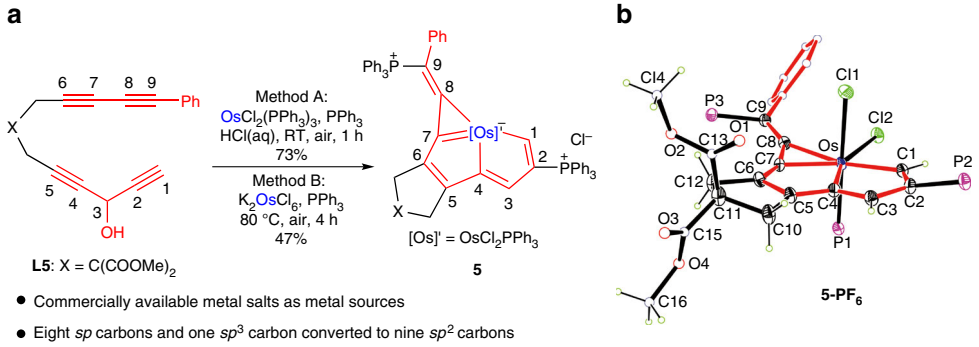

Fig. 3 Synthesis of a CCCC-type chelate from tetrayne and alternative metal sources. **a** Tetrayne as ligand precursor to access a CCCC-type chelate. **b** X-ray structure of the cation of **5-PF$_6$** drawn with 50% probability (phenyl groups in PPh_3 are omitted for clarity). Selected bond distances (Å) and bond angles (deg): Os-C1 2.041(3), Os-C4 2.082(3), Os-C7 2.003(3), Os-C8 2.132(3), C1-C2 1.385(5), C2-C3 1.413(5), C3-C4 1.378(5), C4-C5 1.416(5), C5-C6 1.379(5), C6-C7 1.401(5), C7-C8 1.361(5), C8-C9 1.350(5), Os-C1-C2 118.7(2), C1-C2-C3 114.6(3), C2-C3-C4 112.7(3), C3-C4-Os 118.6(2), C1-Os-C4 75.36(13), Os-C4-C5 118.0(2), C4-C5-C6 113.9(3), C5-C6-C7 111.0(3), C6-C7-Os 123.2(2), C7-Os-C4 73.85(13), Os-C7-C8 76.0(2), C7-C8-Os 65.7(2), C8-Os-C7 38.26(13), C7-C8-C9 143.2(3)

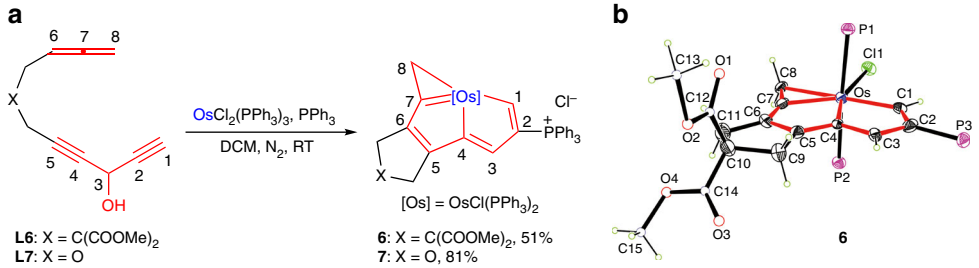

Fig. 4 Synthesis of CCCC-type chelates from allene group substituted diynes. **a** Allene group substituted diynes as ligand precursors to access CCCC-type chelates. **b** X-ray structure of the cation of **6** drawn with 50% probability (phenyl groups in PPh_3 are omitted for clarity). Selected bond distances (Å) and bond angles (deg): Os-C1 2.017(7), Os-C4 2.074(7), Os-C7 2.015(8), Os-C8 2.270(7), C1-C2 1.383(11), C2-C3 1.403(11), C3-C4 1.381(10), C4-C5 1.395 (11), C5-C6 1.385(10), C6-C7 1.349(12), C7-C8 1.403(11), Os-C1-C2 119.1(6), C1-C2-C3 114.4(7), C2-C3-C4 112.8(7), C3-C4-Os 118.0(6), C1-Os-C4 75.7(3), Os-C4-C5 117.9(5), C4-C5-C6 113.8(7), C5-C6-C7 111.4(7), C6-C7-Os 123.4(6), C7-Os-C4 73.4(3), Os-C7-C8 81.1(5), C7-C8-Os 61.3(4), C8-Os-C7 37.6(3)

Os–C single bonds (1.921–2.195 Å) of vinyl osmium complexes (these ranges are based on a search of the Cambridge Structural Database, CSD version 5.38, in November 2016). The carbon–carbon bond distances within the metallacycles (1.366 (10)–1.406(10) Å) lie between the typical single and double carbon–carbon bond distances. The metallabicycle is nearly coplanar, as reflected by the small mean deviation from the least-squares plane (0.020 Å). The planarity of the metallacycles and the carbon–carbon bond distance equivalency indicate extensive electronic delocalization within the osmabicycle ring in **1**. All the salient features of **1** compare well with those of previously reported aromatic osmapentalynes[39]. Osmapentalynes and related osmium chelates with multidentate carbon ligands have attracted considerable attention as novel aromatic molecules with unique properties, especially in the area of photophysics[39–43, 48]. However, previous methods reported for the synthesis of these chelates with multidentate carbon ligands require the use of an unstable osmacycle precursor via standard Schlenk techniques[39–43, 48]. By contrast, triyne **L1** can lead to an osmapentalyne in a one-pot synthesis under an atmosphere of air and from commercially available metal source.

The facile synthesis of **1** using this method demonstrates that it is highly efficient for constructing complexes with three metal–carbon σ bonds via the cyclization of multiyne chains with metal species. To explore the generality of our strategy, we prepared multiynes with different linkers. Similar to **L1**, **L2**–**L4** were able to chelate an osmium center via three metal–carbon σ bonds in a one-pot reaction to achieve CCC-type chelates **2**–**4**, respectively, in high yield (Fig. 2a). These results demonstrate that our method can be applied to a broad range of substrates.

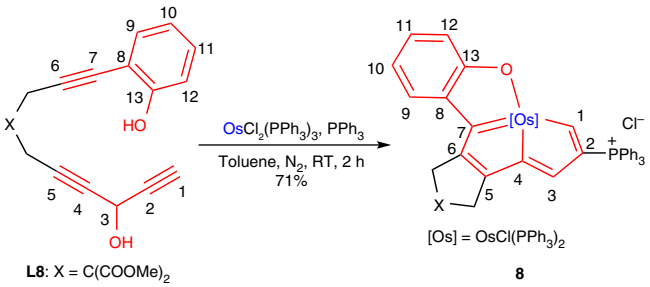

Fig. 5 Synthesis of CCCO-type chelate from a phenolic group substituted triyne. Phenolic group substituted triyne as ligand precursor to access CCCO-type chelate

Extension of the multiyne platform. The efficient ligating ability of **L1**–**L4** inspired us to investigate whether an extension of the multiyne chain will provide tetradentate carbon-ligated chelates and, if so, how the synthesis is achieved.

As shown in Fig. 3a, the reaction of tetrayne **L5** with $OsCl_2(PPh_3)_3$ in air afforded complex **5** with a yield of 73%. The crystal structure of **5-PF$_6$** (the derivative of **5** with PF_6^- as the counteranion) reveals that **5** has a fused metallapentalene

structure with the metallacyclopropenylidene moiety, which is a unique planar tetradentate CCCC-type chelate (Fig. 3b). The metallatricycle is basically coplanar, as reflected by the small mean deviation from the least-squares plane (0.076 Å). The osmium–carbon bond distances within the five-membered metallabicycle (2.041(3) Å for Os–C1, 2.082(3) Å for Os–C4, and 2.003(3) Å for Os–C7) are in agreement with those of osmapentalenes (1.926(6)–2.139(6) Å) reported previously[49], whereas the Os–C8 length is 2.132(3) Å, which is comparable to those of osmium vinyl complexes (1.921–2.195 Å). C8–C9 (1.350(5) Å) is a typical exocyclic double bond. By contrast, the C–C bond distances within the tricyclic skeleton are all between the carbon–carbon single- and double-bond distances, suggesting that there is π-electron delocalization within the fused metallacycle (see Supplementary Fig. 1 for resonance structures). Consistent with the experimental observations, theoretical calculations (natural bond orbital analyses) also indicated that **5** is a tetradentate CCCC-type chelate (Supplementary Fig. 2). It is worth noting that the eight C(*sp*) and one C(sp^3) atoms of **L5** were completely converted into nine C(sp^2) atoms and were incorporated into the final planar conjugated skeleton.

Interestingly, the formation of **5** was also achieved by reacting **L5** with the inorganic salt K_2OsCl_6 under air (Fig. 3a). Although the reactions of triynes **L1**–**L4** with inorganic salts did not work, the reaction of tetrayne **L5** with K_2OsCl_6 indicates that the direct combination of inorganic salts with multiynes could be a readily accessible strategy. This approach may provide opportunities for the use of multiyne chains as carbon ligand precursors; that is extending multiyne chains could enhance their chelating ability, which would lead to the synthesis of useful chelates in an efficient manner.

Multiyne chains with allene groups were also compatible with our strategy. As shown in Fig. 4a, the reaction of **L6** (or **L7**) with $OsCl_2(PPh_3)_3$ led to the formation of complex **6** (or **7**) with a yield of 51% (or 81%). X-ray crystallography analyses confirmed that both **6** (Fig. 4b) and **7** (Supplementary Fig. 6) were tetradentate CCCC-type chelates. The main difference between **5** and **6**/**7** is the hybrid form of C8, which is sp^2-hybridized in **5** but sp^3-hybridized in **6** and **7**.

In addition to all carbon-ligated chelates, chelates with hetero coordination atoms can also be constructed via the cyclization reactions of multiyne chains with metals. As shown in Fig. 5, the reaction of the phenolic group substituted triyne **L8** with $OsCl_2(PPh_3)_3$ afforded the tetradentate CCCO-type chelate **8** with a yield of 71%. **8** was characterized by NMR spectroscopy and all of its characteristic chemical shifts of protons, carbons, and phosphorus were consistent with those of recently reported values for osmapentalenofuran[50]. The structure of **8** was further confirmed by high-resolution mass spectrometry (HRMS), and elemental analyses. It is noteworthy that **8** represents a rare example of a planar tetradentate CCCO-type chelate[50].

DFT studies of the aromaticity of 1–8. Consistent with their structural aromatic characteristics, **1**–**8** exhibit good stability (all of them stable in air at RT). Density functional theory (DFT) calculations were performed to evaluate their aromaticity. Taking **1** as an example, the calculated aromatic stabilization energy (ASE) results are comparable to the values reported for other metallaaromatics (Fig. 6a)[39, 49–54]. We also calculated the nucleus-independent chemical shift (NICS) along the *z*-axis at 1 Å above the ring critical point ($NICS(1)_{zz}$; the average value was used when the environments above and below the ring centers were not equivalent) of model compound **1′**, which we simplified by replacing the PPh_3 groups with PH_3 groups (Fig. 6b)[55–57]. Both the considerable ASE value and negative NICS values suggest that the ring systems in complex **1** are aromatic. The anisotropy of the induced current density (AICD) method[58, 59] was applied to visualize the electron delocalization within the metallacycles (Fig. 6c). The aromatic character was further confirmed by the obvious diatropic ring current (clockwise vectors) within the metallabicyclic moiety of model osmapentalyne **1′**. The $NICS(1)_{zz}$ and ASE values (Table 1; see Supplementary Figs. 8 and 9 for details), and AICD analyses (Supplementary Figs. 11–17) of complexes **2**–**8** are also in good agreement with their aromatic natures. Thus, we propose that the aromaticity of the final products is crucial for the assembly of multiynes with osmium in a one-pot reaction.

Discussion

To characterize the aromaticity-driven processes for multiynes chelating osmium, we performed DFT calculations. The computed free-energy profile of the key steps in the reaction of **L1** with the osmium center to yield the final σ-bonded CCC-type chelate **1** is shown in Fig. 7. The multiyne **L1** may initially bind to the metal to form intermediate **A1** through the dissociation of the

Table 1 Aromaticity evaluations of the cation moieties of complexes 1–8

Complex	NICS(1)zz (ppm) (A/B)	Complex	ASE (kcal/mol)
1′$^+$	−17.3/−14.3	**1**$^+$	29.5
2′$^+$	−17.6/−14.1	**2**$^+$	26.7
3′$^+$	−17.7/−14.3	**3**$^+$	14.6
4′$^+$	−17.2/−15.2	**4**$^+$	20.8
5′$^+$	−13.6/−8.0	**5**$^+$	25.5
6′$^+$	−16.0/−6.8	**6**$^+$	25.8
7′$^+$	−16.2/−6.7	**7**$^+$	14.1
8′$^+$	−17.5/−5.3	**8**$^+$	21.7

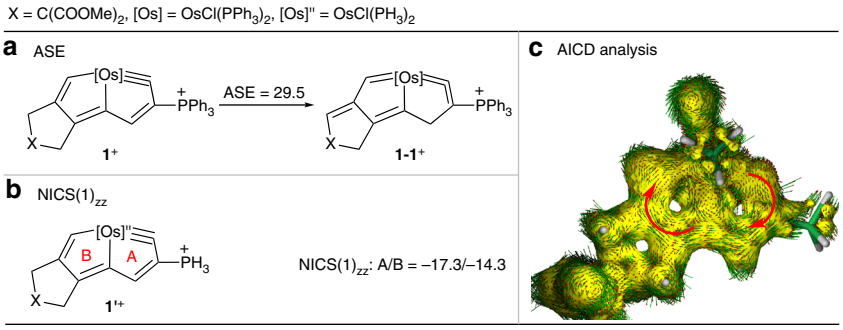

Fig. 6 Aromaticity of the cation moiety of complex **1**. **a** Aromatic stabilization energy (ASE, kcal/mol) evaluations of the aromaticity of the cation moiety of complex **1**. **b** $NICS(1)_{zz}$ (nucleus-independent chemical shift along the *z*-axis at 1 Å above the ring critical point, ppm) evaluations of the aromaticity of the cation moiety of model complex **1′**. **c** Anisotropy of the induced current density (AICD) plot of the cation moiety of model complex **1′** with an isosurface value of 0.025. The magnetic field vector is orthogonal to the ring plane and points upward (aromatic species exhibit clockwise diatropic circulations)

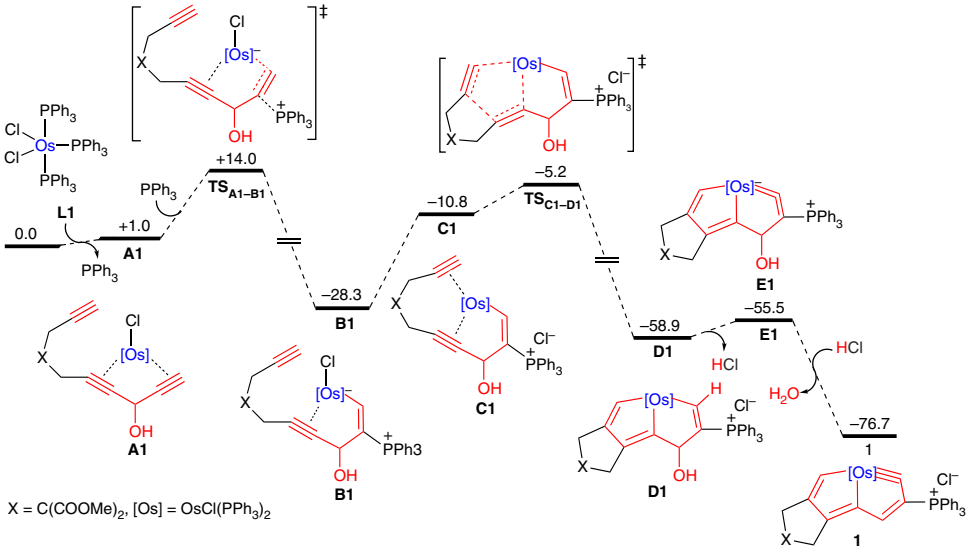

Fig. 7 Gibbs free energy profile for the DFT-calculated formation mechanism of complex **1** at 298 K. The computed free energies are in kcal/mol

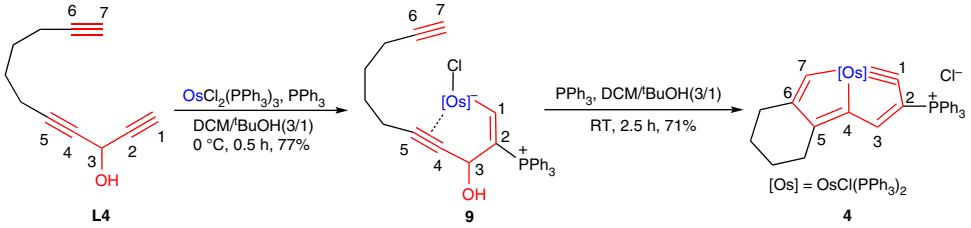

Fig. 8 Isolation of the key intermediate. Isolation of the alkynyl-coordinated osmium vinyl intermediate **9** and its transformation to CCC-type osmium chelate **4**

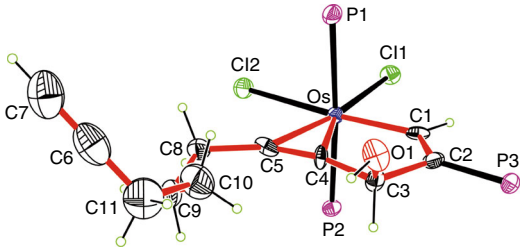

Fig. 9 X-ray molecular structure of complex **9** drawn with 50% probability. Phenyl groups in PPh_3 are omitted for clarity. Selected bond distances (Å) and bond angles (deg): Os-C1 2.019(7), Os-C4 2.153(7), Os-C5 2.220(7), C1-C2 1.373(11), C2-C3 1.524(11), C3-C4 1.480(10), C3-O1 1.397(10), C4-C5 1.248(12), C5-C8 1.473(12), C8-C9 1.546(12), C9-C10 1.532(16), C10-C11 1.565(16), C6-C11 1.487(19), C6-C7 1.28(2), Os-C1-C2 126.0(6), C1-C2-C3 114.4(6), C2-C3-C4 104.6(6), C2-C3-O1 112.4(7), C3-C4-Os 122.4(5), C1-Os-C4 72.6(3), Os-C4-C5 76.4(5), C4-C5-Os 70.5(4), C4-Os-C5 33.1(3), Os-C5-C8 135.4(6), C11-C6-C7 177.6(14)

PPh_3 ligand from the metal center of $OsCl_2(PPh_3)_3$, which was computationally found to be facile. The following nucleophilic addition of PPh_3 to the terminal coordinated acetenyl group leads to the formation of the first metal–carbon σ bond, which could generate the alkynyl-coordinated osmium vinyl intermediate **B1**. This process has an energy barrier of 13.0 kcal/mol and is exergonic by 29.3 kcal/mol. The formation of the other two metal–carbon σ bonds occurs in two steps: the coordination of the remaining terminal C≡C bond with the metal center to form **C1** and [2 + 2 + 1] cyclization to furnish the bicyclic intermediate **D1** (with an energy barrier of 23.1 kcal/mol and exergonic of 30.6 kcal/mol from **B1** to **D1**). Finally, an acid-mediated aromatization can yield the final energetically favorable aromatic product **1** with three metal–carbon σ bonds, which is substantially more stable (by 21.2 kcal/mol) than **E1**. DFT calculations clearly show that the aromatic product **1** is more stable (more than 17 kcal/mol) than all the intermediates, which provides a thermodynamic driving force for the formation of three metal–carbon σ bonds.

The rationality of the aromaticity-driven mechanism was further verified by the isolation of a key intermediate for the synthesis of CCC-type chelate **4**. As shown in Fig. 8, when the reaction of **L4** with $OsCl_2(PPh_3)_3$ was carried out in a mixed solvent of dichloromethane and tert-butanol (3/1, v/v) at 0 °C for 0.5 h, complex **9** was isolated with a yield of 77%. Although **9** is labile in common organic solvents, it can be stable in tetrahydrofuran for weeks. Single-crystal X-ray diffraction (Fig. 9) reveals that **9** is an alkynyl-coordinated osmium vinyl complex with a free terminal C≡C bond, which is consistent with the intermediate **B1** shown in Fig. 7. Other related metal vinyl complexes have also been isolated as intermediates that were demonstrated to be highly reactive[60, 61]. Complex **9** could convert to osmapentalyne **4** when the reaction temperature was increased to RT. As monitored by in situ NMR, the conversion of **L4** to intermediate **9** and finally to chelate **4** further confirms that **9** is a key intermediate in the aromaticity-driven cyclization reaction (see Supplementary Fig. 21 for in situ ^{31}P NMR monitoring spectra). Attempts to capture the corresponding intermediates related to **C1** and **D1** were unsuccessful, probably due to the strong aromaticity driving force of the final product.

In summary, we developed a highly efficient multidentate carbon ligand platform that involves the use of multiyne chains for the preparation of metal chelates with three or more metal–carbon σ

bonds in a one-pot reaction under mild conditions. The multiyne chains consist of two functional modules and a linker, we term which carbolongs. They can be used to react with a commercially available metal complex, or even a simple metal salt, affording all carbon-ligated chelates on the gram scale. Our theoretical and experimental studies revealed that aromaticity-driven processes play a substantial role in the high efficiency and robust characteristics of chelating metals with these multiyne chains. The application of this strategy to utilize various multiynes as a carbon ligand platform will potentially gain widespread use as a promising complement to existing techniques for the preparation of polycyclic organometallic complexes.

Methods

General methods. Details of the synthesis and characterization of the multiynes and transition metal complexes can be found in the Supplementary Information. For X-ray data of complexes **1**, **5-PF$_6$**, **6**, **7**, and **9**, see Supplementary Tables 2, 3. For the detailed crystal structures of complexes **1**, **5-PF$_6$**, **6**, **7**, and **9**, see Supplementary Figs. 3–7. For the mechanisms of the formation of complexes **5**–**8**, see Supplementary Figs. 18–20. For the HRMS, ^{1}H, ^{31}P NMR, and ^{13}C NMR spectra of the complexes in this article, see Supplementary Figs. 22–97. For the thermal decomposition data of complexes **1**–**8**, see Supplementary Table 1. The synthesis procedures for **1**, **5**, **7**, and **8** are representative of those for the preparation of all the described transition metal complexes.

Synthesis of tridentate CCC-type chelate 1. A dichloromethane solution (5 mL) of **L1** (1.20 g, 4.58 mmol) was added slowly to a green solution of $OsCl_2(PPh_3)_3$ (4.01 g, 3.83 mmol) and PPh_3 (5.02 g, 19.1 mmol) in dichloromethane (150 mL) under an air atmosphere, and the reaction mixture was stirred at RT for 1 h to yield a brown solution. The solution was evaporated under vacuum to a volume of ~15 mL and then washed with Et_2O (3 × 200 mL) to afford a brown solid. The solid was purified by flash chromatography on silica gel (eluent: 20:1 dichloromethane/methanol) to yield complex **1** as a brown solid. Yield: 4.05 g, 82%.

Synthesis of tetradentate CCCC-type chelate 5. HCl (1.30 M aqueous solution 146 µL, 0.190 mmol) and a chloroform solution (2 mL) of **L5** (70 mg, 0.193 mmol) were added to a green solution of $OsCl_2(PPh_3)_3$ (200 mg, 0.191 mmol) and PPh_3 (250 mg, 0.953 mmol) in chloroform (10 mL) under an air atmosphere, and the reaction mixture was stirred at RT for 1 h to yield a red solution. The solvent was completely removed under vacuum. The resulting residue was dissolved in chloroform (2 mL) and washed with Et_2O (3 × 20 mL) to afford a red solid, and the solid was purified by column chromatography on silica gel (eluent: 20:1 dichloromethane/methanol) to yield complex **5** as a red solid. Yield: 199 mg, 73%. Please see Supplementary Methods for an alternative method for synthesis of complex **5**.

Synthesis of tetradentate CCCC-type chelate 7. A dichloromethane solution (2 mL) of **L7** (130 mg, 0.802 mmol) was added slowly to a green solution of $OsCl_2(PPh_3)_3$ (550 mg, 0.525 mmol) and PPh_3 (692 mg, 2.64 mmol) in dichloromethane (20 mL). The reaction mixture was stirred at RT for 30 min to yield a brown solution. The solution was evaporated under vacuum to a volume of ~2 mL and washed with Et_2O (3 × 30 mL) to afford a brown solid. The solid was purified by flash chromatography on silica gel (eluent: 20:1 dichloromethane/methanol) to yield complex **7** as a yellow solid. Yield: 506 mg, 81%.

Synthesis of tetradentate CCCO-type chelate 8. A toluene solution (5 mL) of **L8** (570 mg, 1.61 mmol) was added in one portion to a green solution of $OsCl_2(PPh_3)_3$ (1.36 g, 1.30 mmol) and PPh_3 (1.70 g, 6.48 mmol) in toluene (35 mL). The reaction mixture was stirred slowly at RT for 2 h to yield a green precipitate. Complex **8** was obtained as a green solid by filtration and washing with Et_2O (3 × 40 mL). Yield: 1.28 g, 71%.

Computational details. To obtain the ASE values and elucidate the mechanism, we used the original structures without changing the PPh_3 groups to PH_3 groups to obtain a more reasonable estimation of the energy differences. All of these structures evaluated were optimized at the B3LYP/6–31G* level of DFT[62–65] with an SDD basis set[66] to describe P, Cl, and Os atoms; single-point energy calculations were then performed on the mechanism using the TPSS/6-31G* method[67] with the PCM solvation method in dichloromethane[68]. Because we used simplified structures in the other calculations, all of these structures were studied using a larger basis set. The B3LYP/6-311++G** level of DFT[62–65] with a double-ζ valence basis set (LanL2DZ) was used to describe the P, Cl, and Os atoms. Frequency calculations were performed to confirm the characteristics of all the calculated structures as minima. In all calculations, the effective core potentials (ECPs) reported by Hay and Wadt with polarization functions were added for P (ζ(d) = 0.34), Cl (ζ(d) = 0.514), Os (ζ(f) = 0.886)[69]. NICS values were calculated at the B3LYP-GIAO/6-311++G** level. All the above calculations were performed using the Gaussian 09 software package[70]. The AICD calculations were performed using AICD software[58].

Data availability. Data relating to the X-ray crystal structures are available from the Cambridge Crystallographic Data Centre (CCDC) under deposition numbers CCDC 1506325 (**1**), CCDC 1506339 (**5-PF$_6$**), CCDC 1548457 (**6**), CCDC 1548468 (**7**), and CCDC 1548472 (**9**). These data can be obtained free of charge from the Cambridge Crystallographic Date Centre via www.ccdc.cam.ac.uk/data_request/cif. For the XYZ coordinates of the optimized structures in the DFT studies of the aromaticity and mechanism, see Supplementary Data 1 and 2. The authors declare that all other data supporting the findings of this study are available within the article and its Supplementary Information file.

Received: 18 May 2017 Accepted: 8 November 2017
Published online: 04 December 2017

References

1. Crabtree, R. H. *The Organometallic Chemistry of the Transition Metals,* 6th edn (Wiley, Hoboken, 2014).
2. Spessard, G. O. & Miessler, G. L. *Organometallic Chemistry,* 3rd edn (Oxford University Press, New York, 2015).
3. Inoue, A. & Oshima, K. in *Main Group Metals in Organic Synthesis* (eds Yamamoto, H. & Oshima, K.) 51–154 (Wiley-VCH, Weinheim, 2005).
4. Pannell, K. H. & Sharma, H. K. (Cyclopentadienyl)dicarbonylmethyliron ((η^5-C_5H_5)Fe(CO)$_2$CH$_3$, FpMe), a seminal transition-metal alkyl complex: mobility of the methyl group. *Organometallics* **29**, 4741–4745 (2010).
5. Trnka, T. M. & Grubbs, R. H. The development of L_2X_2Ru=CHR olefin metathesis catalysts: an organometallic success story. *Acc. Chem. Res.* **34**, 18–29 (2001).
6. Esteruelas, M. A., López, A. M. & Oliván, M. Osmium-carbon double bonds: formation and reactions. *Coord. Chem. Rev.* **251**, 795–840 (2007).
7. Conejero, S., Paneque, M., Poveda, M. L., Santos, L. L. & Carmona, E. C–H bond activation reactions of ethers that generate iridium carbenes. *Acc. Chem. Res.* **43**, 572–580 (2010).
8. Jia, M. & Ma, S. New approaches to the synthesis of metal carbenes. *Angew. Chem. Int. Ed.* **55**, 9134–9166 (2016).
9. Conejero, S. et al. Monodentate, N-heterocyclic carbene-type coordination of 2,2′-bipyridine and 1,10-phenanthroline to iridium. *Angew. Chem. Int. Ed.* **47**, 4380–4383 (2008).
10. Whited, M. T. & Grubbs, R. H. A catalytic cycle for oxidation of *tert*-butyl methyl ether by a double C–H activation-group transfer process. *J. Am. Chem. Soc.* **130**, 16476–16477 (2008).
11. Castro-Rodrigo, R. et al. Formation of osmium- and ruthenium-cyclobutylidene complexes by ring expansion of alkylidenecyclopropanes. *J. Am. Chem. Soc.* **131**, 15572–15573 (2009).
12. Vivancos, Á. et al. A Diels-Alder reaction triggered by a [4+3] metallacycloaddition. *J. Am. Chem. Soc.* **137**, 4074–4077 (2015).
13. Jia, G. Recent progress in the chemistry of osmium carbyne and metallabenzyne complexes. *Coord. Chem. Rev.* **251**, 2167–2187 (2007).
14. Bolaño, T., Esteruelas, M. A. & Oñate, E. Osmium-carbon multiple bonds: reduction and C–C coupling reactions. *J. Organomet. Chem.* **696**, 3911–3923 (2011).
15. Shi, C. & Jia, G. Chemistry of rhenium carbyne complexes. *Coord. Chem. Rev.* **257**, 666–701 (2013).
16. Heppekausen, J., Stade, R., Goddard, R. & Fürstner, A. Practical new silyloxy-based alkyne metathesis catalysts with optimized activity and selectivity profiles. *J. Am. Chem. Soc.* **132**, 11045–11057 (2010).
17. Chen, J. et al. Conversion of metallabenzynes into carbene complexes. *Angew. Chem. Int. Ed.* **50**, 7295–7299 (2011).
18. Chen, J., Sung, H. H. Y., Williams, I. D., Lin, Z. & Jia, G. Synthesis and characterization of a rhenabenzyne complex. *Angew. Chem. Int. Ed.* **50**, 10675–10678 (2011).
19. Steffen, A., Ward, R. M., Jones, W. D. & Marder, T. B. Dibenzometallacyclopentadienes, boroles and selected transition metal and main group heterocyclopentadienes: synthesis, catalytic and optical properties. *Coord. Chem. Rev.* **254**, 1950–1976 (2010).
20. Yan, X. & Xi, C. Conversion of zirconacyclopentadienes into metalloles: Fagan–Nugent reaction and beyond. *Acc. Chem. Res.* **48**, 935–946 (2015).
21. Ma, W. et al. Metallacyclopentadienes: synthesis, structure and reactivity. *Chem. Soc. Rev.* **46**, 1160–1192 (2017).
22. Steffen, A. et al. 2,5-Bis(*p*-R-arylethynyl)rhodacyclopentadienes show intense fluorescence: denying the presence of a heavy atom. *Angew. Chem. Int. Ed.* **49**, 2349–2353 (2010).
23. Hoyt, J. M., Sylvester, K. T., Semproni, S. P. & Chirik, P. J. Synthesis and electronic structure of bis(imino)pyridine iron metallacyclic intermediates in iron-catalyzed cyclization reactions. *J. Am. Chem. Soc.* **135**, 4862–4877 (2013).
24. Mizukami, Y., Li, H., Nakajima, K., Song, Z. & Takahashi, T. Coupling of titanacyclopentadienes with a Cp ligand and elimination of one substituent. *Angew. Chem. Int. Ed.* **53**, 8899–8903 (2014).

25. Frogley, B. J. & Wright, L. J. A metallaanthracene and derived metallaanthraquinone. *Angew. Chem. Int. Ed.* **56**, 143–147 (2017).
26. Bleeke, J. R. Metallabenzenes. *Chem. Rev.* **101**, 1205–1227 (2001).
27. Landorf, C. W. & Haley, M. M. Recent advances in metallabenzene chemistry. *Angew. Chem. Int. Ed.* **45**, 3914–3936 (2006).
28. Wright, L. J. Metallabenzenes and metallabenzenoids. *Dalton Trans.* **15**, 1821–1827 (2006).
29. Bleeke, J. R. Aromatic iridacycles. *Acc. Chem. Res.* **40**, 1035–1047 (2007).
30. Paneque, M., Poveda, M. L. & Rendón, N. Synthesis and reactivity of iridacycles containing the $TpMe_2Ir$ moiety. *Eur. J. Inorg. Chem.* **2011**, 19–33 (2011).
31. Dalebrook, A. F. & Wright, L. J. in *Advances in Organometallic Chemistry,* Vol. 60 (eds Anthony, F. H. & Mark, J. F.) 93–177 (Academic, New York, 2012).
32. Chen, J. & Jia, G. Recent development in the chemistry of transition metal-containing metallabenzenes and metallabenzynes. *Coord. Chem. Rev.* **257**, 2491–2521 (2013).
33. Cao, X.-Y., Zhao, Q., Lin, Z. & Xia, H. The chemistry of aromatic osmacycles. *Acc. Chem. Res.* **47**, 341–354 (2014).
34. Fernández, I., Frenking, G. & Merino, G. Aromaticity of metallabenzenes and related compounds. *Chem. Soc. Rev.* **44**, 6452–6463 (2015).
35. Pugh, D. & Danopoulos, A. A. Metal complexes with 'pincer'-type ligands incorporating N-heterocyclic carbene functionalities. *Coord. Chem. Rev.* **251**, 610–641 (2007).
36. Poyatos, M., Mata, J. A. & Peris, E. Complexes with poly(N-heterocyclic carbene) ligands: structural features and catalytic applications. *Chem. Rev.* **109**, 3677–3707 (2009).
37. Hopkinson, M. N., Richter, C., Schedler, M. & Glorius, F. An overview of N-heterocyclic carbenes. *Nature* **510**, 485–496 (2014).
38. Sattler, A. & Parkin, G. A new class of transition metal pincer ligand: tantalum complexes that feature a $[CCC]_X$3-donor array derived from a terphenyl ligand. *J. Am. Chem. Soc.* **134**, 2355–2366 (2012).
39. Zhu, C. et al. Stabilization of anti-aromatic and strained five-membered rings with a transition metal. *Nat. Chem.* **5**, 698–703 (2013).
40. Zhu, C. et al. σ-Aromaticity in an unsaturated ring: osmapentalene derivatives containing a metallacyclopropene unit. *Angew. Chem. Int. Ed.* **54**, 3102–3106 (2015).
41. Zhu, C. et al. CCCCC pentadentate chelates with planar Möbius aromaticity and unique properties. *Sci. Adv.* **2**, e1601031 (2016).
42. Zhu, C. et al. Synthesis and characterization of a metallacyclic framework with three fused five-membered rings. *Angew. Chem. Int. Ed.* **56**, 9067–9071 (2017).
43. Luo, M. et al. Reactions of isocyanides with metal carbyne complexes: isolation and characterization of metallacyclopropenimine intermediates. *J. Am. Chem. Soc.* **139**, 1822–1825 (2017).
44. Tanaka, K. (ed.) *Transition-Metal-Mediated Aromatic Ring Construction* (Wiley, Hoboken, 2013).
45. Jia, G. Progress in the chemistry of metallabenzynes. *Acc. Chem. Res.* **37**, 479–486 (2004).
46. Jia, G. Our journey to the chemistry of metallabenzynes. *Organometallics* **32**, 6852–6866 (2013).
47. Frogley, B. J. & Wright, L. J. Fused-ring metallabenzenes. *Coord. Chem. Rev.* **270**, 151–166 (2014).
48. Zhu, C. et al. Five-membered cyclic metal carbyne: synthesis of osmapentalynes by the reactions of osmapentalene with allene, alkyne, and alkene. *Angew. Chem. Int. Ed.* **54**, 7189–7192 (2015).
49. Zhu, C. et al. Planar Möbius aromatic pentalenes incorporating 16 and 18 valence electron osmiums. *Nat. Commun.* **5**, 3265 (2014).
50. Lu, Z. et al. Metallapentalenofurans and lactone-fused metallapentalynes. *Chem. Eur. J.* **23**, 6426–6431 (2017).
51. Mauksch, M. & Tsogoeva, S. B. Demonstration of "Möbius" aromaticity in planar metallacycles. *Chem. Eur. J.* **16**, 7843–7851 (2010).
52. Hao, Y., Wu, J. & Zhu, J. σ Aromaticity dominates in the unsaturated three-membered ring of cyclopropametallapentalenes from groups 7–9: a DFT study. *Chem. Eur. J.* **21**, 18805–18810 (2015).
53. Wei, J. et al. Aromatic dicupra[10]annulenes. *J. Am. Chem. Soc.* **138**, 60–63 (2016).
54. Zhang, Y. et al. Spiro metalla-aromatics of Pd, Pt, and Rh: synthesis and characterization. *J. Am. Chem. Soc.* **139**, 5039–5042 (2017).
55. Schleyer, Pv. R., Maerker, C., Dransfeld, A., Jiao, H. & Hommes, N. J. Rv. E. Nucleus-independent chemical shifts: a simple and efficient aromaticity probe. *J. Am. Chem. Soc.* **118**, 6317–6318 (1996).
56. Chen, Z., Wannere, C. S., Corminboeuf, C., Puchta, R. & Schleyer, P. v. R. Nucleus-independent chemical shifts (NICS) as an aromaticity criterion. *Chem. Rev.* **105**, 3842–3888 (2005).
57. Fallah-Bagher-Shaidaei, H., Wannere, C. S., Corminboeuf, C., Puchta, R. & Schleyer, Pv. R. Which NICS aromaticity index for planar π rings is best? *Org. Lett.* **8**, 863–866 (2006).
58. Herges, R. & Geuenich, D. Delocalization of electrons in molecules. *J. Phys. Chem. A* **105**, 3214–3220 (2001).
59. Geuenich, D., Hess, K., Köhler, F. & Herges, R. Anisotropy of the induced current density (ACID), a general method to quantify and visualize electronic delocalization. *Chem. Rev.* **105**, 3758–3772 (2005).
60. Xia, H. et al Osmabenzenes from the reactions of HC≡CCH(OH)C≡CH with $OsX_2(PPh_3)_3$ (X=Cl, Br). *J. Am. Chem. Soc.* **126**, 6862–6863 (2004).
61. Zhuo, Q. et al. Synthesis of fused metallaaromatics via intramolecular C–H activation of thiophenes. *Organometallics* **35**, 1497–1504 (2016).
62. Hay, P. J. & Wadt, W. R. Ab initio effective core potentials for molecular calculations. Potentials for K to Au including the outermost core orbitals. *J. Chem. Phys.* **82**, 299–310 (1985).
63. Lee, C., Yang, W. & Parr, R. G. Development of the Colle-Salvetti correlation-energy formula into a functional of the electron density. *Phys. Rev. B* **37**, 785–789 (1988).
64. Miehlich, B., Savin, A., Stoll, H. & Preuss, H. Results obtained with the correlation energy density functionals of Becke and Lee, Yang and Parr. *Chem. Phys. Lett.* **157**, 200–206 (1989).
65. Becke, A. D. Density-functional thermochemistry. III. The role of exact exchange. *J. Chem. Phys.* **98**, 5648–5652 (1993).
66. Peng, C., Ayala, P. Y., Schlegel, H. B. & Frisch, M. J. Using redundant internal coordinates to optimize equilibrium geometries and transition states. *J. Comput. Chem.* **17**, 49–56 (1996).
67. Tao, J., Perdew, J. P., Staroverov, V. N. & Scuseria, G. E. Climbing the density functional ladder: nonempirical meta-generalized gradient approximation designed for molecules and solids. *Phys. Rev. Lett.* **91**, 146401 (2003).
68. Scalmani, G. & Frisch, M. J. Continuous surface charge polarizable continuum models of solvation. I. General formalism. *J. Chem. Phys.* **132**, 114110 (2010).
69. Huzinaga, S. (ed.) *Gaussian Basis Sets for Molecular Calculations* (Elsevier, Amsterdam, 1984).
70. Frisch, M. J. et al. *Gaussian 09, revision B.01* (Gaussian, Inc., Wallingford CT, 2009).

Acknowledgements

This research was supported by the National Natural Science Foundation of China (Nos. 21490573 and 21332002) and Project funded by China Postdoctoral Science Foundation (No. 2016M602069). We thank Prof. Zhenyang Lin (Hong Kong University of Science and Technology), Prof. Qiyu Zheng (National Natural Science Foundation of China), Prof. Michael M. Haley (University of Oregon), and Prof. Roald Hoffmann (Cornell University) for their helpful advice on the preparation of this manuscript.

Author contributions

H.X. conceived the project. Q.Z., J.L., X.Z., Y.S. and S.C. performed the experiments. Q. Z., J.L., Y.S. and S.C. recorded all NMR data. Q.Z. and Z.C. solved all X-ray structures. Q. Z., H.Z. and H.X. analysed the experimental data. H.Z. conceived the theoretical work. Y. H. and X.Z. conducted the theoretical work. J.Z., H.Z., Q.Z., Y.H., X.Z. and H.X. analysed and interpreted the computational data. H.Z., Q.Z. and H.X. drafted the paper, with support from Y.H., X.Z. and J.Z. All the authors discussed the results and contributed to the preparation of the final manuscript.

Additional information

Supplementary Information accompanies this paper at https://doi.org/10.1038/s41467-017-02120-z.

Competing interests: The authors declare no competing financial interests.

Reprints and permission information is available online at http://npg.nature.com/reprintsandpermissions/

Publisher's note: Springer Nature remains neutral with regard to jurisdictional claims in published maps and institutional affiliations.

Open Access This article is licensed under a Creative Commons Attribution 4.0 International License, which permits use, sharing, adaptation, distribution and reproduction in any medium or format, as long as you give appropriate credit to the original author(s) and the source, provide a link to the Creative Commons license, and indicate if changes were made. The images or other third party material in this article are included in the article's Creative Commons license, unless indicated otherwise in a credit line to the material. If material is not included in the article's Creative Commons license and your intended use is not permitted by statutory regulation or exceeds the permitted use, you will need to obtain permission directly from the copyright holder. To view a copy of this license, visit http://creativecommons.org/licenses/by/4.0/.

© The Author(s) 2017